Performance analysis of bridge monitoring with the integrated GPS, BDS and GLONASS

Ruijie Xi[1,2], Xiaolin Meng[2], Weiping Jiang[3], Qiyi He[2], Xiangdong An[3]

[1] School of Geodesy and Geomatics, Wuhan University, 129 Luoyu Road, Wuhan 430079, China, (rjxi@whu.edu.cn)
[2] Nottingham Geospatial Institute, The University of Nottingham, Nottingham NG7 2TU, United Kingdom, (xiaolin.meng@nottingham.ac.uk, qiyi.he@nottingham.ac.uk)
[3] GNSS Research Center, Wuhan University, 129 Luoyu Road, Wuhan 430079, China, (wpjiang@whu.edu.cn, xdan@whu.edu.cn)

Key words: *Integration of GPS; BDS and GLONASS; Bridge deformation monitoring; Monitoring precision; Elevation cutoff; Vibration testing.*

ABSTRACT

In present, Global Navigation Satellite System (GNSS) technology has been widely applied as an essential part of a SHM system. With the BeiDou Navigation Satellite System (BDS) becoming available in Asian-Pacific region and the full operation of the GLONASS system, multi-constellation GNSS tend to be the best choice in the SHM systems. The paper presents an SHM experiment on the Baishazhou Yangtze River Bridge in Wuhan, China with the integrated GPS, BDS and GLONASS observations to analyze its performance. Firstly, the precision metrics that a single GNSS system, the integration of two systems and the combined GPS/BDS/GLONASS could be achieved are compared with the bridge monitoring data. It shows that, with more satellites available and the strongest satellite geometry, the combined GPS/BDS/GLONASS gives the highest precision, with 1-2 mm horizontal and 2-5 mm vertical precision. Then, with the integration of GPS/BDS/GLONASS, different elevation cutoffs are set to figure out the best elevation cutoff in the data processing in the bridge monitoring application. The results demonstrate that the precision in horizontal component can always achieve to 1-2 mm level with the rising of cutoff elevation angles, and when the cutoff angle of 40° is selected, the vertical precision would reduce from 5 mm to 7 mm. A vibration test was carried out in the experiment. It shows that the noise level of the solutions from the integrated GPS/BDS/GLONASS is the lowest, which can greatly benefit the modal parameter estimation.

I. INTRODUCTION

Modern societies are heavily dependent upon bridges to keep the transport operation and then to support healthy social and economic development (Farrar and Worden, 2012). However, in the real world, bridges especially the large-scale ones, are often built in earthquake prone areas and river estuary, and have to endure extreme weather conditions. Many of bridges currently stand the progressively increasing traffic volume under inevitable aging. In addition, with the new design and incorporate novel materials coming up, the performance and feasibility of these new structural systems are barely studied (Meng et al., 2011). These circumstances demand that the potential damages should be detected at the earliest time to keep the bridge operating well and to prevent and reduce the losses of lives and property. On august 14 2018, an over 50's year old bridge in Genoa, Italy, collapsed, which made at least 41 death, because of lacking of monitoring systems and regular maintenance. However, just 20 days before, on July 27 2018, the collapse of Minjiang Bridge in Sichuan, China, caused no death and property loss, just because the bridge monitoring system showed the large displacement and the bridge manager made the timely decision to close the bridge. Therefore, the establishment of Structural Health Monitoring (SHM) system is extremely important to monitor the performance of bridges and help the bridge owners to make timely and right decisions.

Global Navigation Satellite System (GNSS) now is widely involved in high-precision Structural Health Monitoring (SHM) applications of bridges, high-rise buildings, dams and other civil engineering infrastructures, due to the appealing advantages comparing with the traditional bridge monitoring sensors (Yu et al., 2016a; Meng et al., 2007; Yi et al., 2013; Yu et al., 2014; Yu et al., 2016b; Meng et al., 2016). For instance, it can provide continuous, all weather, automated positioning solutions, and, with the technological advent of GNSS receivers, the sampling rate can even achieve up to 100 Hz (Yi et al., 2013; Tamura et al., 2002). Among the GNSS systems, the feasibility of GPS used in bridge health monitoring has been fully studied. More than 7 visible GPS satellites at any time and lower than 6 of dilution of precision (DOP) could support the precision of 10 mm in horizontal and 20 mm in vertical component in a dynamic mode (Meng et al., 2004). However, there are still many problems exist in the bridge deformation

monitoring application with GPS technology (Elnabwy et al., 2013; Psimoulis and Stiros, 2008; Psimoulis et al., 2008; Górski, 2017). For instances, cables, supporting towers and passing vehicles could block the GPS signal to dramatically reduce the number of tracked GPS satellites and weaken the satellite geometry in least square resolution of data processing. In addition, the multipath effects, cycle slips caused by the surrounding blockages and the residual atmospheric delay in lower satellites could be heavier. All of these factors will significantly restrict the usage of GPS in the application of bridge deformation monitoring.

In recent years, with the establishment of BeiDou Navigation Satellite System (BDS) and Galileo Navigation Satellite System (Galileo), and the modernization of Global Positioning System (GPS) and GLObalnaya NAvigazionnaya Sputniovaya Sistema (GLONASS), the observable navigation satellites have been extremely increased and the satellite geometry strength is also enhanced (Shi et al., 2013; Pan et al., 2017; Tian et al., 2019; Li et al., 2019; Li et al., 2018). In present, more than 100 navigation satellites in total are available to be observed and they all broadcast multiple frequencies to provide more observables and also make it convenient for error processing (Roberts et al., 2017). Much research efforts have been put into the integration of multi-GNSS observation including real-time kinematic (RTK) positioning, Precise Point Positioning (PPP) and single point positioning (SPP). It is concluded that, with the multi-GNSS observables integration, the positioning precision could improve by nearly over 30% comparing with the results from single GNSS system in different positioning mode (Pan et al., 2017). Therefore, the rise of multi-GNSS integration processing will undoubtedly strengthen the capability of GNSS in the deformation monitoring area. However, the benefits involving positioning precision and stability improvement offered by multi-GNSS in the bridge engineering have not been explored yet (Roberts et al., 2017).

In this case, the paper consists of the following contents: the satellite visibility and Position Dilution of Precision (PDOP) statements are evaluated firstly; a set of real-life bridge monitoring data with GPS, BDS and GLONASS observations is applied to assess the performance of multi-GNSS for bridge monitoring; and the latest conclusions.

II. SATELLITE VISIBILITY AND PDOP EVALUATION OF MULTI-GNSS

As previously mentioned, there are four completed and under construction global navigation satellite systems available, GPS, Galileo, BDS and GLONASS (Li et al., 2018). The satellite constellation statement of these satellite systems can be simply found from Lin et al. (2018). In present, more than 80 navigation satellites can be tracked globally and provide high performance of positioning, navigation and timing services. Figure 1 shows the trajectory of satellite point on the ground on April 26th 2018. It can be seen that compared with the single GNSS system, the combined GNSS covers a larger global scale and the density of satellite is significantly improved.

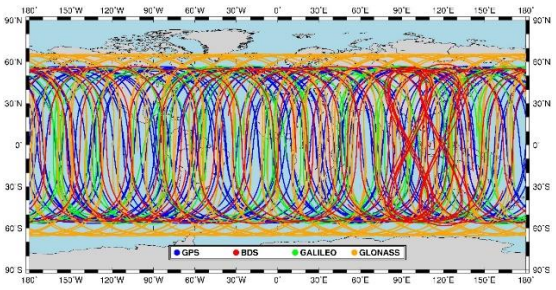

Figure 1. Ground trajectory of satellite point of GPS, BDS, Galileo and GLONASS on April 26th 2018.

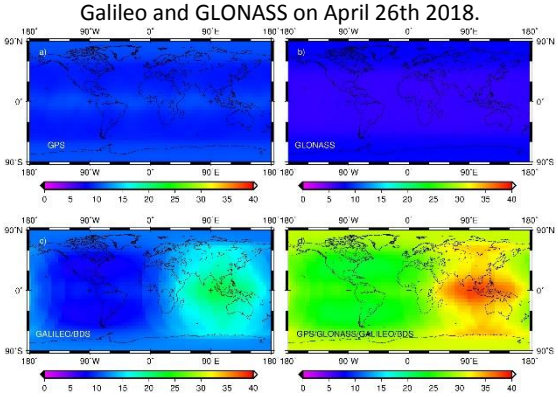

Figure 2. The satellite visibility of GPS, GLONASS, Galileo/BDS and four GNSS systems integrated.

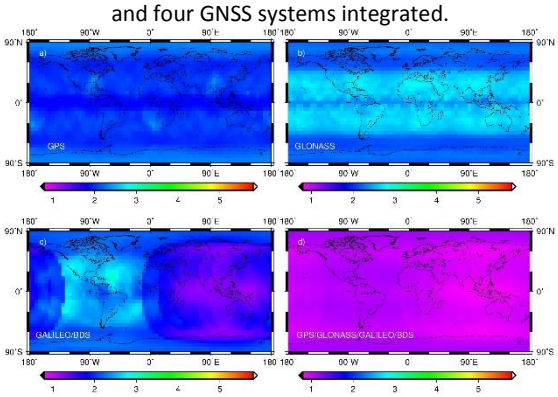

Figure 3. Global distribution of PDOP values of GPS, GLONASS, Galileo/BDS and combined four GNSS systems.

Then, with the broadcast ephemeris on April 26th 2018, we calculated the average number of visible satellites over the whole global scale for four different combination cases, shown in Figure 2. In Figure 2, the satellite elevation mask was set to 10°, and the sampling interval was 5 minutes. The space resolution of global coverage was 5° by 2.5° along latitude and longitude and the altitude was 25m. It is shown that, almost 10 or less GPS-only and GLONASS-only satellites can be observed at one point in the whole global scale. For Galileo and BDS which are under construction, 15-25 satellites are visible in the Asian-Pacific region, due to the enhancement of GEO and IGSO satellite of BDS. For other area, the visibility is significantly reduced, with only 10-15. However, for the one with four system

integration, one can observed that more than 20 satellites are visible at any point in the whole global scale, and in the Asian-Pacific region, the figure can even reach to 40.

III. MULTI-GNSS INTEGRATION POSITIONING METHOD

Generally, the GNSS satellite transfers pseudorange and carrier phase signals for the purpose of positioning and navigation. Since the pseudorange is easily contaminated by multipath and hardware delays, biases are significant. Thus, in bridge deformation monitoring application, only carry phase observations are applied to calculate the displacements (Xi et al., 2018a). The original dual-frequency GNSS phase observation model can be expressed as follows:

$$\begin{aligned}\phi^{i}_{m,p} &= \rho^{i}_{p} + c\left(dt_{p} - dt^{i}\right) + T^{i}_{m,p} - I^{i}_{m,p} \\ &+ \lambda_{m}\left(N^{i}_{m,p} + B_{m,p} - B^{i}_{m}\right) + \varepsilon^{i}_{m,p}\end{aligned} \tag{1}$$

where the superscript i indicates the satellite; subscripts m and p are the frequency number and the station. ϕ_m respresents the carrier phase observation of frequency m in meters; λ_m is the wave length of frequency m (m); ρ resprsents the geometric distance between satellite and receiver antenna (m); c is the speed of light in vacuum (m); dt_p and dt^i indicate the receiver and satellite clock offsets (m), respectively; T and I denote the tropospheric and ionospheric delays (m), respectively. N is the ambiguity in integer cycle. $B_{m,p}$ and B^{i}_{m} are the receiver and satellite related hardware delays in cycles respectively. ε is the observation noise of carrier phase measurement (m).

Generally, the short baselines are often used to achieve a millimeter level accuracy in deformation monitoring application. Under such circumstances, the double difference (DD) technology can reasonably eliminate the common delays between a pair of satellites simultaneous tracked by two GNSS receivers (Xi et al., 2018a, 2018b, 2018c). For GPS, BDS and Galileo systems, who transfer signals in code division multiple access (CDMA) mode, the double differential observation can be simply expressed as follow:

$$\nabla\Delta\phi^{ij}_{m,pq} = \nabla\Delta\rho^{ij}_{pq} + \lambda_{m}\nabla\Delta N^{ij}_{m,pq} + \nabla\Delta\varepsilon^{ij}_{m,pq} \tag{2}$$

where j and q represent the pivot satellite and base station respectively, and $\nabla\Delta$ denotes the DD operator. From Eq. (2), we can see that the common terms such as the receiver, satellite clock offsets, tropospheric and ionospheric delays are cancled by DD. Thus, only position parameters of monitoring station and integer ambiguities terms are in the estimation parameter list (Xi et al., 2018c).

However, for GLONASS system, the different satellites hold the different signal frequency. Thus, the DD observations cannot be formed as other systems did. If we define and as pivot and non-pivot satellite respectively, the single difference (SD) observations of monitoring and reference stations (p and q) are:

$$\begin{aligned}\Delta\phi^{k}_{m,pq} &= \Delta\rho^{k}_{pq} + c\Delta dt_{pq} + \lambda^{k}_{m}\left(\Delta N^{k}_{m,pq} + \Delta B^{k}_{m,pq}\right) + \Delta\varepsilon^{k}_{m,pq} \\ \Delta\phi^{l}_{m,pq} &= \Delta\rho^{l}_{pq} + c\Delta dt_{pq} + \lambda^{l}_{m}\left(\Delta N^{l}_{m,pq} + \Delta B^{l}_{m,pq}\right) + \Delta\varepsilon^{l}_{m,pq}\end{aligned} \tag{3}$$

where Δ denotes the SD operator. From Eq. (3), we can see that the satellite related clock offsets and hardware biaes are eliminated. The tropospheric and ionospheric delays are also weakened significantly to a negligible level. Then, the double difference observation can be formulated and organized as

$$\begin{aligned}\Delta\phi^{k}_{m,pq} - \Delta\phi^{l}_{m,pq} &= \nabla\Delta\rho^{kl}_{pq} + \lambda^{k}_{m}\left(\nabla\Delta N^{kl}_{m,pq} + \nabla\Delta B^{kl}_{m,pq}\right) \\ &+ \lambda^{k}_{m}\left(1 - \frac{\lambda^{l}_{m}}{\lambda^{k}_{m}}\right)\left(\Delta N^{l}_{m,pq} + \Delta B^{l}_{m,pq}\right) + \nabla\Delta\varepsilon^{kl}_{m,pq}\end{aligned} \tag{4}$$

From Eq. (4), we can see that the ambiguity and receiver hardware are divided to two terms, a double differenced and a single differenced of the pivot satellite. Research indicate that the receiver hardware delay can be ignored for the receivers from same manufactures (Wanninger, 2012). For $\Delta N^{l}_{m,pq}$, according to the wavelength of GLONASS, the coefficient $\left(1 - \frac{\lambda^{l}_{m}}{\lambda^{k}_{m}}\right)$ has a range of ±0.0046 (Gao et al., 2015). Thus, the bias in $\Delta N^{l}_{m,pq}$ will have a very small effect on the DD model. In this study, the single difference of Geometry-Free (GF) and Melbourne-Wübbena (MW) combinations are applied to resolve $\Delta N^{l}_{m,pq}$ (Xi et al., 2018c). Taken the consideration of dual-frequency of GLONASS, the approach to obtain the SD ambiguity with SD GF and MW combinations ($\Delta\phi_{GF}$ and $\Delta\phi_{MW}$) is:

$$\begin{cases}\Delta\hat{N}_{1,pq} = \frac{9}{2}\Delta\phi_{MW} - \frac{7}{2}\Delta\phi_{GF} \\ \Delta\hat{N}_{2,pq} = \frac{7}{2}\Delta\phi_{MW} - \frac{7}{2}\Delta\phi_{GF}\end{cases} \tag{5}$$

and the float resolution will be good enough for the positioning. Therefore, Eq. (4) can be reformulated as

$$\Delta\phi^{k}_{m,pq} - \Delta\phi^{l}_{m,pq} = \nabla\Delta\rho^{kl}_{pq} + \lambda^{k}_{m}\nabla\Delta N^{kl}_{m,pq} + \nabla\Delta\varepsilon^{kl}_{m,pq} \tag{6}$$

Under such circumstance, the double difference observation of GLONASS Eq. (4) can be solved together with GPS, BDS and Galileo systems. A Kalman Filter (KF) will be used to estimate the positioning parameters and float ambiguities and we use the LAMBDA method to fix the float ambiguities. For more details regarding the data processing procedure, please see Xi et al. (2018a).

IV. EXPERIMENTS AND RESULTS

A. *Data description*

For assessment of multi-GNSS deformation monitoring on bridges, the experiment data were collected at Baishazhou Yangtze River Bridge in Wuhan, China. It is a cable-stayed highway bridge links Wuchang

and Hanyang over the Yangtze River. It was designed and constructed in 1997, and it is 3586 m long, 28.5 m wide with the main span of 618 m.

An episodic trail was carried out on the bridge on September 26. The monitoring stations were set-up on the middle span (S012, S035), top of the towers (S023, S029) and the bridge piers (W009, H001). A reference station was located on the bridge management building near the bridge. The distribution of stations on the bridge is shown in Figure 4. All the stations were equipped with ComNav-K508 receiver board and antennas, which support tracking GPS, BDS and GLONASS satellites. In the experiment, the sampling rate of receivers on middle span and towers was set to 10 Hz, and on the piers 1 Hz. The detailed information of the stations is listed in Table 1.

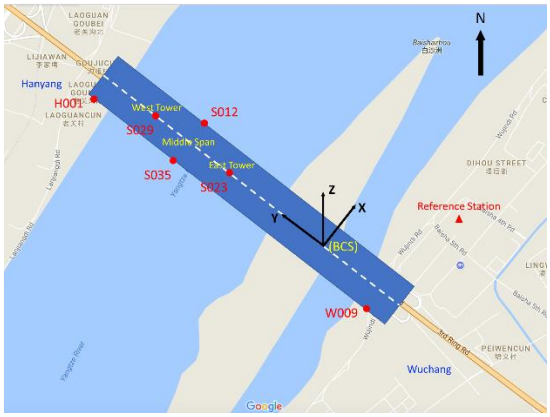

Figure 4. Monitoring stations set-up on the bridge (The background figure is from Google Earth). A Bridge Coordinate System (BCS) was defined by this paper (X and Y denotes to lateral and longitudinal direction of the bridge, and Z is orthogonal with the plane of X and Y and denotes to the height direction).

Table 1 The information of monitoring stations.

Station Name	Location	Baseline Length (m)	Sampling Rate (Hz)	Receivers
S012	Middle Span	2480.40	10	ComNav-K508
S035	Middle Span	2476.09	10	ComNav-K508
S023	East Tower	2173.45	10	ComNav-K508
S029	West Tower	2789.62	10	ComNav-K508
H001	Pier	3075.53	1	ComNav-K508
W009	Pier	1439.11	1	ComNav-K508

The data were collected continuously for 16 hours from 8:00 to 24:00 (UTC). Then, a home-made multi-GNSS data processing and analysis software package was applied to analyze the current GNSS constellation and provide the positioning resolution in RTK mode.

B. *Satellite visibility and PDOP analysis*

Figure 5 illustrates the satellite visibility and PDOP variations at different elevation cutoffs (from 10° to 40° at an interval of 10°) over the 16 hours on the bridge. In Figure 5, it gives the results of all the possible system combinations. It shows that, for the single systems without multi-constellation GNSS combination, four to ten satellites can be tracked during the experimental session at 10° cutoff angle, and the fluctuation of PDOP is mostly between two and four. However, for GLONASS system, when the satellites are less than five, the PDOP value will increase dramatically larger than six. In this case, the stability of deformation monitoring using GLONASS-only system would not be guaranteed. For the two system combination counterparts, the trackable satellites increase to ten to twenty, and the PDOP values are fairly stable at about two. However, the GPS/BDS/GLONASS combination can track even more than 30 satellites sometimes, and the PDOP value is rather close to one all the time. It means that the positioning precision and stability will not be influenced by the geometry change of GPS/BDS/GLONASS combination positioning.

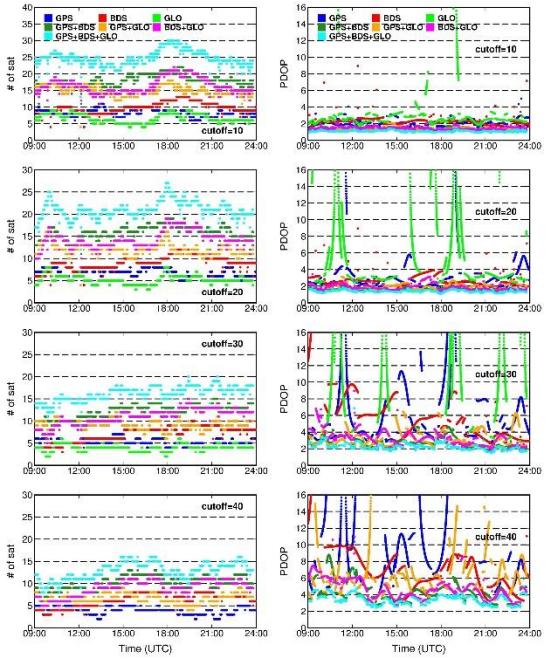

Figure 5. Satellite visibility and PDOP values at different elevation cutoffs for the stations on the bridge.

With the increasing of cutoff elevation angle, the satellite visibility decreases gradually, about five GNSS satellites reducing for per 10° rise. When the cutoff elevation is 20° and 30°, the PDOP value fluctuates around two. Under cutoff elevation of 40°, there are still eight to sixteen GPS/BDS/GLONASS satellites are available and the PDOP value is always less than 6. That means the sound positioning solutions would be still achievable with GPS/BDS/GLONASS combined observations at cutoff elevation of 40°.

C. *Positioning precision analysis with multi-GNSS combination observations*

Since the stations on the pier (W009 and H001) are much stable than others, we assumed that the stations are static in a relative short time. In this case, the data processing results of these two stations can be applied to see the benefits of precision improvement with multi-GNSS combination observations. Therefore, firstly, we selected the data for only one hour (September 27th 2016, 2:00-3:00) when the traffic volume was not heavy. Though the experimental session is short, the data quantity is enough for comparing purpose and generally one hour is usually as a unit for time series analysis for bridge statement assessment (Meng et al., 2018). Figure 6 shows the sky-plot of these two stations in this hour. Apparently, more than 20 GNSS satellites can be observed during this session. From Figure 5, we know that this could be the normal satellite constellation statement with GPS/BDS/GLONASS combination.

Based on the home-made data processing software with the multi-GNSS integration method mentioned above, we obtained the GNSS data processing results for every possible system combination. After moving the average value from the time series, the baseline residual is plotted in Figure 7. In order to show the universal precision of GNSS positioning precision, the results of North (N), East (E) and Height (U) directions in the station local coordinate frame are shown in the figure instead of Bridge Coordinate System. It also notes that the baseline lengths of W009-BASE and H001-BASE are 1.5 km and 3.0 km respectively.

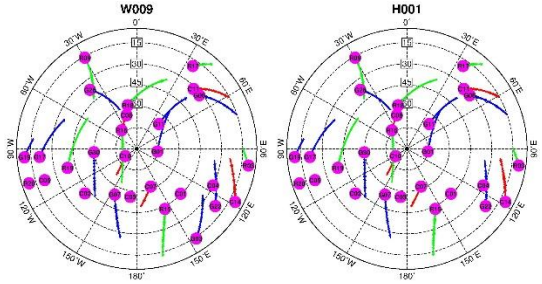

Figure 6. Sky-plot of stations on the bridge.

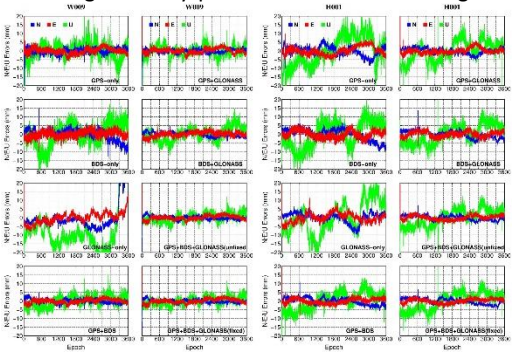

Figure 7. Baseline residual errors of data processing after moving average values. The results of individual single GNSS system, the combination of two systems and the combination of GPS/BDS/GLONASS with unfixed ambiguity of GLONASS (unfixed) and fixed (fixed) are all shown in the figure.

In Figure 7, it can be seen from the residual time series that, in general, the result from the combination of GPS/BDS/GLONASS is slightly better than any combination of the two systems and the individual single system shows the worst regardless of W009 and H001. Among the three GNSS systems, GLONASS-only seems give a much unstable series because the satellite visibility of it is not always applicable for the positioning. For the two systems combination, they have an almost same positioning performance. For the results of GPS/BDS/GLONASS combination, it shows that the fluctuation of time series in horizontal direction is always within 5 mm, except for the large values caused by instantaneous vehicle passing at H001. For W009, mostly the time series in vertical direction is also within 5 mm. However, the vertical time series of H001 is mostly out of 5 mm. That is because the baseline length of H001 is longer than W009, the DD residual tropospheric and ionospheric delays cannot be fully canceled, which will have a larger influence on the vertical direction. To clearly show the precision performance, we calculated the Standard Deviation (STD) statistics in Table 2. From the table, we can see that the GPS/BDS/GLONASS could be the best choice in the deformation monitoring applications, with 1-2 mm in horizontal component for baseline length less than 3 km, and better than 3 mm for 1.5 km and 5 mm for 3 km baselines.

Table 2 STD of data processing results for different system combinations. (mm)

Station		GPS (G)	BDS (C)	GLO (R)	GC	GR	CR	GCR
W009	N	1.8	3.1	-	1.2	1.1	1.3	1.0
	E	2.2	2.0	-	1.3	1.8	1.5	1.4
	U	5.0	6.4	-	3.1	3.3	3.8	2.4
H001	N	2.7	3.3	-	1.9	1.7	2.1	1.4
	E	2.5	2.3	-	1.6	1.8	1.7	1.3
	U	8.6	7.4	-	5.0	5.8	5.5	5.0

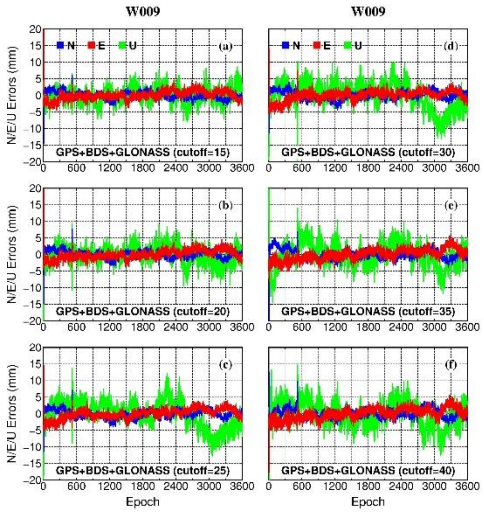

Figure 8. Baseline residual errors of data processing with GPS/BDS/GLONASS combination observations at different

cutoff elevation angles (range from 15 to 40 for per 5°) for W009.

In addition, generally the elevation cutoff is set to 10°, and we know that the observations from low elevation satellite suffer from the residual tropospheric delays and multipath effects. In this case, the positioning resolution would also be affected by these unmodeled errors. However, on the contrary, the low elevation satellite plays a key role in enhancing the satellite geometry. Under such cases, the elevation cutoff should be carefully set for a high precision and reliable positioning resolution. However, with the rising of multi-GNSS positioning, the available satellites are significantly increased and the PDOP value is also at an acceptable level, which can be confirmed from Figure 5. Therefore, with the GPS/BDS/GLONASS integration observations, we processed the data at different elevation cutoffs from 15° to 40° for per 5°. The results are shown in Figure 8 and Figure 9.

It can be observed that, with the rising of elevation cutoffs, the time series in N and E directions have a very subtle change regardless W009 and H001. The residual errors are still within 5 mm. However, for the vertical direction, the time series become unstable gradually. The maximum residual errors have exceeded 10 mm and 20 mm for W009 and H001 respectively when the cutoff elevation is 40°.

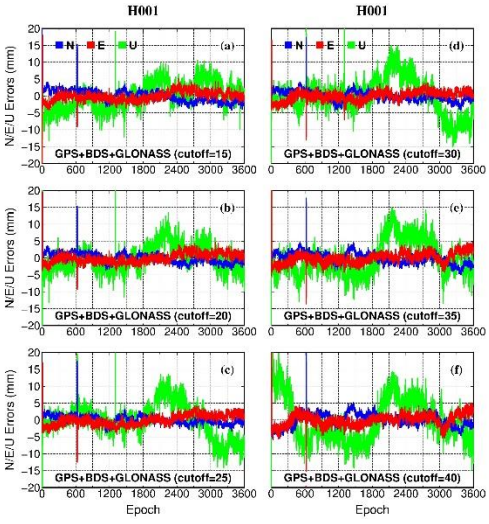

Figure 9. Baseline residual errors of data processing with GPS/BDS/GLONASS combination observations at different cutoff elevation angles (range from 15 to 40 for per 5°) for H001.

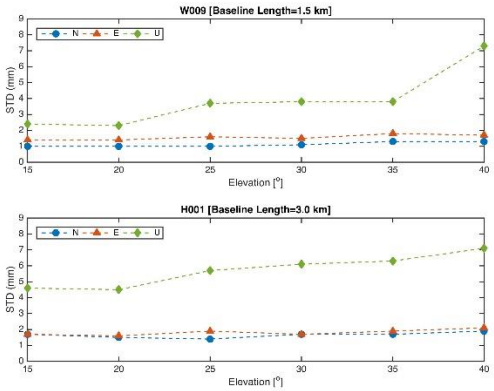

Figure 10. STD statistics of baselines resolution for W009 and H001 at different elevation cutoffs.

Figure 10 gives the STD statistics of multi-GNSS positioning under different elevation cutoffs. One can clearly observe that the positioning precisions in N and E directions keep at a level of better than 2 mm. The precision in U directions, however, reduces from 3-5 mm to about 7 mm, due to the worse satellite geometry in height directions. However, compared with the single system positioning in Table 2, it can still achieve to the precision level of individual single system. The results demonstrate the great benefits of multi-GNSS positioning bring into on deformation monitoring applications.

D. *Dynamic testing*

In this section, the monitoring data on the middle span and top of the towers of the bridge will be applied to see the performance of multi-GNSS positioning in dynamic mode. Due to the huge data quantity of 10 Hz sampling rate, the results for arbitrary 10 min are shown in Figure 11. In the figure, the positioning results have been transformed to the Bridge Coordinate System as shown in Figure 4.

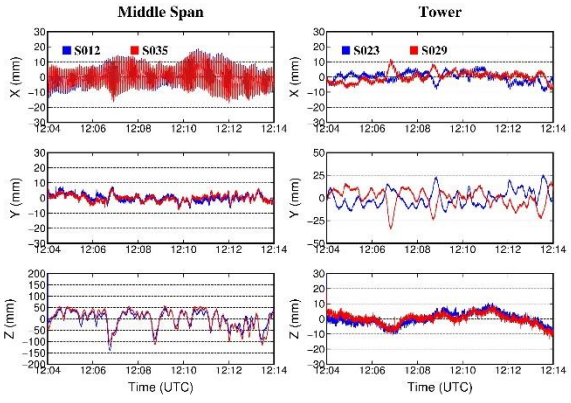

Figure 11. Vibration time series of middle span and top of the towers for 10 min.

It shows that there is a high frequency vibration signal in the X direction of the middle span. The amplitude can reach up to 20 mm sometimes. The significant movements happened in the Z direction, larger than 15 centimetres. This could be the responses caused by the traffic excitations such as the lorries passing by. In addition, the two stations on the middle span show a

similar movement during the experimental session. For the towers, the movements are mainly in X and Y directions, and they seem show an opposite movement trend. Compared with the time series in Z direction of middle span, the tower in Y direction has the same pattern. That is because the vibration of middle span in height can derive the movement of two towers in longitudinal direction by cables. The time series in Z direction show an obvious low frequency signal and the fluctuation is only within 10 mm. This could be the multipath effect and residual tropospheric delays reflected in the positioning results (Wang et al., 2017). More research could be done for residual tropospheric delays effect under the significant height difference between reference and monitoring stations in the future.

Figure 12 gives the Fast Fourier Transform (FFT) analysis of vibration time series of S035 and S029. S012 and S023 have the same results with the corresponding stations. For the comparing purpose, in the figure, the GPS-only, combination of GPS and BDS, and GPS/BDS/GLONASS combination results are shown, since the GPS and GPS/BDS hold the best performance in the respective system combination results in Figure 7. We can see that all the three results can clearly reflect the mode frequency of the bridge. These are 0.226 Hz in the lateral direction, 0.2883 Hz in the height direction, and 0.35 Hz for the towers (Huang et al., 2005; Zhang et al., 1998). Still because of the cables, the natural frequency of middle span in height is also shown in the towers. In addition, the GPS/BDS/GLONASS combination always has the lowest noise level in the whole frequency band. Though the better extent is slight, this could be beneficial for the small amplitude vibration frequency extraction in the bridge dynamic monitoring application (Moschas and Stiros, 2011, 2014, Breuer et al., 2015). This could be another benefits that multi-GNSS integrated positioning in the deformation monitoring application.

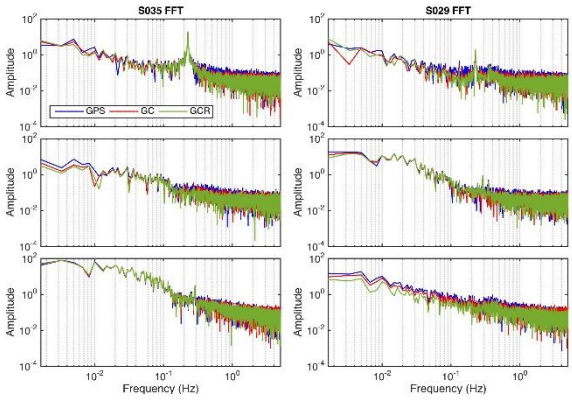

Figure 12. The FFT analysis results of vibration time series for middle span and top of the tower.

V. Conclusion

The paper presents an SHM experiment on the Baishazhou Yangtze River Bridge in Wuhan, China with the integrated GPS, BDS and GLONASS observations to analyse its performance. Firstly, the precision metrics that a single GNSS system, the integration of two systems and the combined GPS/BDS/GLONASS could be achieved are compared with the bridge monitoring data. It shows that, with more satellites available and the strongest satellite geometry, the combined GPS/BDS/GLONASS gives the highest precision, with 1-2 mm horizontal and 2-5 mm vertical precision. Then, with the integration of GPS/BDS/GLONASS, different elevation cutoffs are set to figure out the best elevation cutoff in the data processing in the bridge monitoring application. The results demonstrate that the precision in horizontal component can always achieve to 1-2 mm level with the rising cutoff elevation angles, and when the cutoff angle of 40° is selected, the vertical precision would reduce from 5 mm to 7 mm. A vibration test was carried out in the experiment. It shows that the noise level of the solutions from the integrated GPS/BDS/GLONASS is the lowest, which can greatly benefit the modal parameter estimation.

VI. Acknowledgements

This research was supported by the National Natural Science Foundation of China (Grant Nos. 41525014, 41304007 and 41210006), the Program for Changjiang Scholars of the Ministry of Education of China. The Chinese Scholarship Council (CSC) has provided the first author a scholarship which allows him to visit the University of Nottingham for two years to research and study in the UK from November 2016. ESA is acknowledged for sponsoring GeoSHM feasibility a Demo project.

References

Breuer P., Chmielewski T., Górski P., et al. Monitoring horizontal displacements in a vertical profile of a tall industrial chimney using Global Positioning System technology for detecting dynamic characteristics[J]. Structural Control and Health Monitoring, 2015, 22(7): 1002-1023.

Elnabwy M. T., Kaloop M. R., Elbeltagi E. Talkha steel highway bridge monitoring and movement identification using RTK-GPS technique[J]. Measurement, 2013, 46(10): 4282-4292.

Farrar C.R., Worden K. Structural health monitoring: a machine learning perspective[M]. John Wiley & Sons, 2012.

Gao W., Gao C., Pan S. A method of GPS/BDS/GLONASS combined RTK positioning for middle-long baseline with partial ambiguity resolution[J]. Survey Review, 2015, 49:354, 212-220.

Górski P. Dynamic characteristic of tall industrial chimney estimated from GPS measurement and frequency domain decomposition[J]. Engineering Structures, 2017, 148: 277-292.

Huang S., Wu W., Li P. GPS Dynamic Monitoring Experiment and Analysis of Long-Span Cable-Stayed Bridge[J]. Geomatics and Information Science of Wuhan University, 2005, 30(11): 999-1002.

Li X., Li X., Liu G., et al. Triple-frequency PPP ambiguity resolution with multi-constellation GNSS: BDS and Galileo[J]. Journal of Geodesy, 2019(360).

Li X., Li X., Yuan Y., et al. Multi-GNSS phase delay estimation and PPP ambiguity resolution: GPS, BDS, GLONASS, Galileo[J]. Journal of Geodesy, 2018, 92:579-608.

Meng X., Gogoi N., Dodson A. H., et al. Using multi-constellation GNSS and EGNOS for bridge deformation monitoring[C]//Proceedings of the joint international symposium on deformation monitoring. Hong Kong, China. 2011: 2-4.

Meng X., Dinh N., Xie Y., et al. Design and Implementation of a New System for Large Bridge Monitoring—GeoSHM[J]. Sensors, 2018, 18(3):775.

Meng X., Dodson A. H., Roberts G.W. Detecting bridge dynamics with GPS and triaxial accelerometers[J]. Engineering Structures, 2007, 29(11): 3178-3184.

Meng X., Xie Y., Bhatia P, et al. Research and development of a pilot project using GNSS and Earth observation (GeoSHM) for structural health monitoring of the Forth Road Bridge in Scotland[J]. 2016.

Meng, X., Roberts, G. W., Dodson, A. H., et al. Impact of GPS satellite and pseudolite geometry on structural deformation monitoring: analytical and empirical studies. Journal of Geodesy. 2004, 77(12), 809-822.

Moschas F., Stiros S. Three-dimensional dynamic deflections and natural frequencies of a stiff footbridge based on measurements of collocated sensors[J]. Structural Control and Health Monitoring, 2014, 21(1): 23-42.

Moschas F., Stiros S. Measurement of the dynamic displacements and of the modal frequencies of a short-span pedestrian bridge using GPS and an accelerometer[J]. Engineering Structures, 2011, 33(1): 10-17.

Pan L., Zhang X., Li X., et al. Satellite availability and point positioning accuracy evaluation on a global scale for integration of GPS, GLONASS, BeiDou and Galileo[J]. Advances in Space Research, 2017:S0273117717305392.

Psimoulis P., Stiros S. Experimental assessment of the accuracy of GPS and RTS for the determination of the parameters of oscillation of major structures[J]. Computer-Aided Civil and Infrastructure Engineering, 2008, 23(5): 389-403.

Psimoulis P., Pytharouli S., Karambalis D., et al. Potential of Global Positioning System (GPS) to measure frequencies of oscillations of engineering structures[J]. Journal of Sound and Vibration, 2008, 318(3): 606-623.

Roberts G. W., Tang X. The use of PSD analysis on BeiDou and GPS 10Hz dynamic data for change detection[J]. Advances in Space Research, 2017, 59(11): 2794-2808.

Shi C., Zhao Q., Hu Z., et al. Precise relative positioning using real tracking data from COMPASS GEO and IGSO satellites[J]. GPS solutions, 2013, 17(1): 103-119.

Tamura Y., Matsui M., Pagnini L. C., et al. Measurement of wind-induced response of buildings using RTK-GPS[J]. Journal of Wind Engineering and Industrial Aerodynamics, 2002, 90(12): 1783-1793.

Tian Y., Sui L., Xiao G., et al. Analysis of Galileo/BDS/GPS signals and RTK performance[J]. GPS Solutions, 2019, 23(2): 23-37.

Wang D., Meng X., Gao C., et al. Multipath extraction and mitigation for bridge deformation monitoring using a single-difference model[J]. Advances in Space Research, 2017, 60(12): 2882-2895.

Wanninger L. Carrier-phase inter-frequency bias of GLONASS receivers. Journal of Geodesy, 2012, 86(2), 139-148.

Xi R., Chen H., Meng X., Jiang W., Chen Q. Reliable dynamic monitoring of bridges with integrated GPS and BeiDou[J]. Journal of Surveying Engineering. 2018a, 144(4): 04018008.

Xi R., Jiang W., Meng X., et al. Bridge monitoring using BDS-RTK and GPS-RTK techniques[J]. Measurement, 2018b, 120: 128-139.

Xi R., Meng X., Jiang W., et al. GPS/GLONASS carrier phase elevation-dependent stochastic modelling estimation and its application in bridge monitoring[J]. Advances in Space Research, 2018c, 62(9): 2566-2585.

Yi T., Li H., Gu M. Experimental assessment of high-rate GPS receivers for deformation monitoring of bridge[J]. Measurement, 2013, 46(1): 420-432.

Yi T., Li H., Gu M. Recent research and applications of GPS-based monitoring technology for high-rise structures[J]. Structural Control and Health Monitoring, 2013, 20(5): 649-670.

Yu J., Meng X., Shao X., et al. Identification of dynamic displacements and modal frequencies of a medium-span suspension bridge using multimode GNSS processing[J]. Engineering Structures, 2014, 81: 432-443.

Yu J., Shao X., Yan B., et al. Research and Development on Global Navigation Satellite System Technology for Bridge Health Monitoring[J]. China Journal of Highway and Transport, 2016a, 29(4): 30-41.

Yu J., Yan B., Meng X., et al. Measurement of bridge dynamic responses using network-based real-time kinematic GNSS technique[J]. Journal of Surveying Engineering, 2016b, 142(3): 04015013.

Zhang J., Li L. Aseismic and wind-resistant analysis for Wuhan Baishazhou Yangtze River Bridge[J]. Bridge Construction, 1998, 3: 8-12.